Building and Environment 284 (2025) 113468

Contents lists available at ScienceDirect

Building and Environment

journal homepage: www.elsevier.com/locate/buildenv

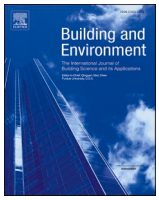

Incorporating lateral bypass in the design of horizontal permeable reactive barriers (HPRBs) for chlorinated vapor intrusion mitigation

Nicolò Tonolo, Clarissa Settimi, Daniela Zingaretti, Renato Baciocchi, Iason Verginelli *

Department of Civil Engineering and Computer Science Engineering, University of Rome Tor Vergata, Via del Politecnico 1, Rome 00133, Italy

ARTICLE INFO

Keywords:
Chlorinated solvents
Numerical model
Permeable reactive barriers
Chlorinated vapor intrusion
Risk mitigation

ABSTRACT

Horizontal Permeable Reactive Barriers (HPRBs) installed in the unsaturated zone beneath buildings recently emerged as promising passive strategies to mitigate chlorinated vapor intrusion at contaminated sites. To date, experimental investigations have been conducted only at the laboratory scale. To progress toward full-scale implementation, modeling tools are essential for barrier design and predicting field performance. Existing modeling approaches assume infinitely wide barriers failing to account for the potential lateral bypass of vapors around the barrier. This assumption hinders the accurate assessment of field performance, as vapors may still reach buildings through longer diffusion pathways. In this work a 2-D numerical model that incorporates both vertical and horizontal dimensions of the reactive barrier was developed in Comsol Multiphysics. The results highlight that vapor lateral bypass is a critical factor. Barriers twice the width of the building footprint may achieve attenuation factors in the order of 10^{-3}, providing adequate protection only for low contamination levels (slightly above MCLs). For higher contamination scenarios, additional vertical barriers are required to intercept lateral vapors. This study explores several configurations using purely horizontal barriers or integrating them with reactive vertical layers or HDPE liners. The latter solutions are capable of achieving attenuation factors in the order of 10^{-10}, ensuring acceptable indoor risk for various chlorinated solvents, even under saturated groundwater conditions. To support the selection and design of barrier configurations, this study provides a set of nomographs as practical tools tailored to the target subsurface vapor attenuation levels, facilitating the field-scale implementation of this mitigation approach.

1. Introduction

Chlorinated solvents contamination is a concerning and widespread environmental issue [1–3]. These compounds are often detected as pollutants in soil, groundwater and surface water due to their extensive use or improper disposal in the past [2,4–6]. If released in the subsurface, chlorinated solvents are generally low biodegradable and persist as dense non-aqueous phase liquids (DNAPL), overpassing the saturated zone and contaminating groundwater with diffuse and persistent plumes [7–9]. From groundwater and subsurface DNAPL sources, the contamination by chlorinated solvents can extend into the unsaturated zone through volatilization [1,10–12]. Also, if buildings are present, vapors can reach the indoor environment through vapor intrusion (VI), posing critical concerns for human health [13–19]. In sites affected by chlorinated solvents diffuse contamination, mitigation techniques that manage VI pathway are more indicated and sustainable than traditional remediation for technical and economic reasons [20,21]. In such cases, different existing mitigation techniques can be adopted to manage VI risks, including active techniques (e.g., sub-slab depressurization systems or air conditioning control) or passive techniques (e.g., low permeable barriers) [22–26]. In this context, the use of reactive layers, specifically Horizontal Permeable Reactive Barriers (HPRBs), aimed at passively degrading chlorinated vapors in the subsurface has been proposed as a novel mitigation strategy for managing VI [21,27,28]. The advantage of HPRBs relies on the capacity to transform vapors of harmful compounds, such as trichloroethylene (TCE) or tetrachloroethylene (PCE), into less toxic ones due to the induction of degradation reactions by the reactive filling material [29–31]. HPRBs were investigated in previous literature by experiments and modeling aimed at understanding the feasibility of using different reactive filling materials, such as oxidants or reducing agents, and the preliminary design of the technique. Mahmoodlu et al. [27,29] proposed the use of dry solid

* Corresponding author.
E-mail address: verginelli@ing.uniroma2.it (I. Verginelli).

https://doi.org/10.1016/j.buildenv.2025.113468
Received 29 May 2025; Received in revised form 14 July 2025; Accepted 20 July 2025
Available online 21 July 2025

granules of potassium permanganate ($KMnO_4$) as constituents for HPRBs to promote chlorinated solvents oxidation to CO_2, testing its potential in degrading TCE vapors at partially saturated conditions in laboratory batch and column tests and showing its effectiveness towards the treatment. Based on the experimental results obtained with $KMnO_4$, Verginelli et al. [28] described the HPRB behavior by developing a 1-D analytical model at steady-state, showing that a barrier less than 1 m thick can mitigate chlorinated solvent vapors at acceptable levels for a timeframe of 10 years. However, the dissolution of solid $KMnO_4$ could occur due to water leaching, leading to the consumption of the barrier and making it a low-lasting technique [28].

To overcome this problem, zero-valent iron (ZVI) was proposed as a filling material, able to induce the degradation of chlorinated solvents by reductive dehalogenation to mainly non-carcinogenic hydrocarbons [21,31]. Different ZVI-based reactive materials were investigated as constituents for HPRBs, particularly micrometric ZVI [21,31], ZVI bimetals [30,32], and sulfidated ZVI bimetals [33]. In these studies, TCE vapor degradation batch tests were performed at different conditions (i.e., different humidity and aerobic/anaerobic conditions). Micrometric ZVI was found suitable to fill HPRBs and effective towards TCE vapors degradation [21,31,34,35]. The addition of nickel (Ni) or copper (Cu) onto ZVI enhanced dechlorination via electron transfer and hydrogenation reactions, leading to faster TCE vapors removal [30,32]. However, due to passivation, both ZVI and bimetals ensured limited treatment efficiency in time [33]. Sulfidated ZVI-based bimetals instead showed resistance to passivation and enhanced dechlorination of TCE vapors in batch and column tests, thus resulting in the most promising alternatives for constituting HPRBs [33]. Based on the experimental results and simple 1-D analytical solutions, the minimum HPRB thickness needed to ensure good levels of TCE reduction was estimated in the order of 1 m [21] for ZVI and 12–18 cm for ZVI bimetals and sulfidated materials [32,33].

More advanced modeling evaluations on HPRBs were recently explored by assuming oxidant-based barriers. Wang et al. [36] and Zhu et al. [37] developed 2-D multilayer analytical and numerical models considering the effect of several environmental factors (e.g., pH, saturation level, temperature, non-homogeneity of the source concentration), barrier properties (e.g., vertical thickness, adsorption on reactive material) and distance from the source of contamination. Also, Shi et al. [38] developed a multilayer 1-D analytical model that considers advection due to pressure gradients and potential biodegradation affecting vapor transport in the soil and the reactive layer. The mentioned studies confirmed that a less than 1 m thick barrier could ensure effective chlorinated vapors degradation, and increasing HPRB thickness and saturation levels lead to enhanced degradation performances [36–38].

However, existing models assume an infinitely wide barrier in the horizontal direction, thus neglecting the possibility of lateral vapor bypass. This assumption significantly limits their applicability for field-scale design, as it overlooks the potential for vapors to migrate around the edges of the barrier and reach overlying buildings through longer diffusion pathways.

Given these limitations, this study presents a 2-D steady-state numerical model implemented in Comsol Multiphysics, specifically conceived to support the design of HPRBs as a vapor intrusion mitigation strategy. The developed model explicitly incorporates both vertical and lateral dimensions of the barrier, allowing for the evaluation of bypass phenomena and providing a more realistic assessment of barrier performance at contaminated sites. To this aim, four different configurations of HPRBs were investigated to determine the most effective design for mitigating chlorinated vapor intrusion. The considered configurations include: (1) a purely horizontal continuous barrier, (2) a horizontal funnel and gate configuration with the alternation of reactive material and low permeable layers and (3–4) a belting configuration (i.e., horizontal and vertical layers surrounding the building in the subsurface) made either entirely of reactive material or combining it with a vertical low-permeability layer. The aim of this study is to deepen the HPRB design and provide indications of the vapors attenuation expected in buildings using this technique. Hence, indications on the expected performances for different HPRB configurations are provided in order to support full-scale implementation and facilitate field application at contaminated sites.

2. Model development

2.1. Vapor transport governing equations

The transport of contaminated vapors in the porous media was modeled at steady-state conditions, assuming a purely diffusive transport in homogenous soil (Eq. (1)) and a diffusive-reactive transport in the HPRB (Eq. (2)):

$$\nabla\cdot(D_s\nabla c) = 0 \tag{1}$$

$$\nabla\cdot(D_{HPRB}\nabla c) \; - \; k\cdot c = 0 \tag{2}$$

where c (g/m^3) represents the contaminant concentration in the vapor phase, k (s^{-1}) is the degradation rate constant in the vapor phase, and D_s (m^2/s) and D_{HPRB} (m^2/s) are respectively the effective diffusion coefficients in the soil and in the HPRB. Note that this assumption is consistent with previous modeling studies showing that, on a long-term average basis, diffusion can be considered the dominant transport process for the migration of gases in the vadose zone [39,40].

The effective diffusion coefficients in the soil and in the HPRB, D_s and D_{HPRB}, were obtained from the Millington and Quirk equation [41], as reported in Eq. (3) and Eq. (4), respectively:

$$D_s = \frac{D_a\cdot\left(\theta_{e,s}-\theta_{w,s}(z)\right)^{3.33}}{\theta_{e,s}^2} + \frac{D_w\cdot\theta_{w,s}(z)^{3.33}}{H\cdot\theta_{e,s}^2} \tag{3}$$

$$D_{HPRB} = \frac{D_a\cdot\theta_{a,HPRB}^{3.33}}{\theta_{e,HPRB}^2} + \frac{D_w\cdot\theta_{w,HPRB}^{3.33}}{H\cdot\theta_{e,HPRB}^2} \tag{4}$$

where D_a (m^2/s), D_w (m^2/s) and H (-) are, respectively, the air and water diffusion coefficients and the dimensionless Henry's constant of the contaminant.

In Eq. (3), $\theta_{e,s}$ (-) and $\theta_{w,s}$ (-) are the effective porosity and the volumetric water content of the soil, respectively. $\theta_{w,s}$ was calculated as a function of the vertical distance from the water table (z) using the Van Genuchten equation [42]:

$$\theta_{w,s}(z) = \theta_{r,s} + \frac{\theta_{e,s} \; - \; \theta_{r,s}}{\left[1+(a\cdot z)^n\right]^m} \tag{5}$$

where z (m) is the vertical distance above the groundwater level, $\theta_{r,s}$ (-) is the residual water content of the soil and a (m^{-1}), n (-), m (-) are the soil hydraulic retention parameters in the Van Genuchten equation [43].

In Eq. (4), $\theta_{a,HPRB}$ (-), $\theta_{w,HPRB}$ (-) and $\theta_{e,HPRB}$ (-) are respectively the air content, the water content and the effective porosity of the HPRB, assumed to be fixed in the reactive layer.

Since the degradation of the compounds takes place in the water phase within the barrier porosity, the kinetic rate constants in the vapor phase (k) used in the transport equation (Eq. (2)) can be expressed, assuming linear equilibrium partitioning, as follows [21,44]:

$$k = k_1\cdot\frac{\theta_{w,HPRB}}{H} \tag{6}$$

where k_1 (s^{-1}) is the first-order kinetic degradation constant in the water phase. A first-order kinetic was commonly observed in degradation tests of chlorinated compounds in both aqueous and gaseous phases when using reducing agents such as ZVI-based materials [21,33,45,46]. Alternative kinetic models have also been reported, including zero-order (k_0, $g/m^3/s$) for bimetallic reducing materials [32,33] and second-order

(k_2, g/m^3/s) for oxidant-based systems [27–29]. These can be approximated as pseudo-first-order kinetics assuming either a constant initial contaminant concentration for zero-order systems, or a constant oxidant concentration for second-order reactions [28,32]. In general, the kinetic degradation constant is specific to the reactive material used and can be determined through laboratory tests on a representative compound.

2.2. Numerical implementation

An axial-symmetric 2-D steady-state numerical model was developed using the software Comsol Multiphysics (Comsol Inc., Burlington, MA, Version 6.0), employing the software module "transport of diluted species in porous media" to model both the diffusion of chlorinated vapors in the subsurface (Eq. (1)) and the diffusive-reactive transport in the domain regions representing the HPRB (Eq. (2)).

The domain considered for developing the model is depicted in Fig. 1 and consisted of a building located above a soil layer, where a HPRB system was implemented to mitigate vapor intrusion. The building is assumed to have a foundation with a depth H_b and a width L_b. The underlying soil extends laterally for a width L_s and vertically down to the contaminated groundwater table, located at depth H_{gw}.

The HPRB system was modeled with four different design configurations to evaluate how variations in geometry affect vapor attenuation in the subsurface, particularly with respect to potential lateral vapor bypass (Fig. 1).

Specifically, Configuration 1 represents the simplest design, consisting solely of a HPRB with a thickness d_{HPRB} and width L_{HPRB}, placed 1 m below the building foundations. This configuration is intended to intercept vapors rising vertically from the subsurface, not including any specific elements to limit lateral vapor migration.

Configuration 2 builds upon the first configuration by adding a non-permeable horizontal layer made of high-density polyethylene (HDPE), 1 mm thick (d_{HDPE}) and L_{HDPE} wide, extending laterally from the HPRB corners. This impermeable layer is designed to reduce the risk of lateral vapor bypass by extending the effective width of the barrier system.

Configuration 3 introduces a more robust solution to lateral bypass by incorporating a vertical barrier made of the same reactive material used in the HPRB. This vertical barrier, with a height H_{PRB}, extends from the end of the horizontal HPRB up to the ground surface, effectively surrounding the building footprint and creating a containment zone.

Finally, Configuration 4 adopts a similar approach to Configuration 3 but replaces the reactive vertical barrier with a 1 mm thick HDPE liner.

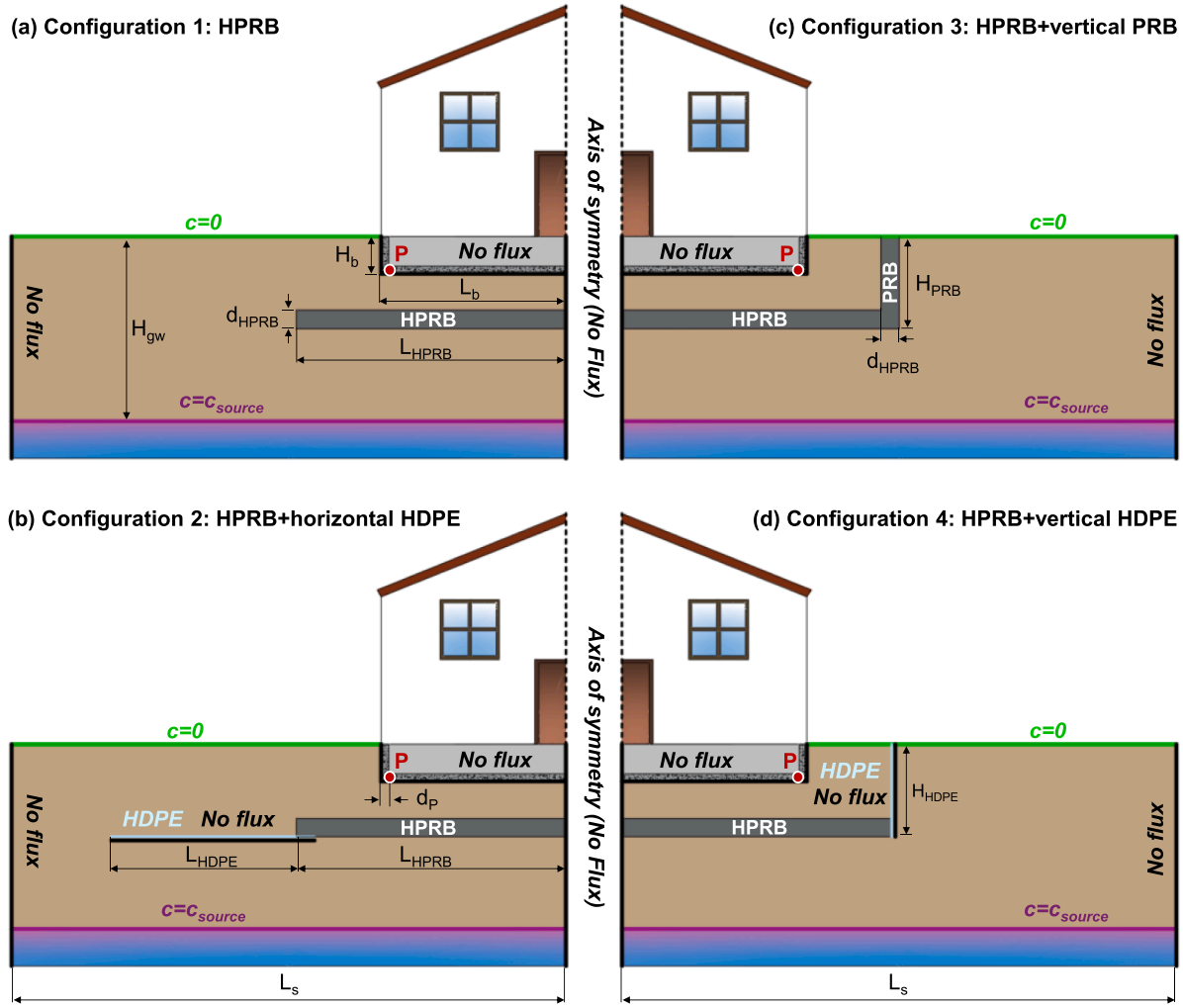

Fig. 1. Representation of the different domains assumed for the developed numerical model for each configuration proposed. In the first two configurations, only horizontal barriers were considered, consisting of either (a) reactive permeable material (HRPB) or (b) reactive material combined with an HDPE liner. In the remaining two configurations, the horizontal barriers were coupled with vertical barriers made of either (c) reactive material (PRB) or (d) HDPE liner. Boundary conditions are graphically represented, consisting of concentration boundary in the source of contamination (purple lines) and in the soil surface (green lines) and no flux condition (black lines). Point P (red dot) represents the point of evaluation of soil vapor attenuation for each specific HPRB system configuration. Light blue lines represent the problem domain in which a 1 mm thick HDPE liner was considered.

This configuration aims to physically block lateral vapor flow using an impermeable material rather than relying on chemical reactivity.

As boundary conditions in the model, a constant concentration equal to c_{source} was imposed along the entire domain width at the depth of the groundwater table (c=c_{source}, purple line in Fig. 1), while a zero concentration condition was applied at the segment representing the ground surface ($c = 0$, green line in Fig. 1). Note that the assumption of a continuous and spatially unconfined vapor source is a conservative assumption, representing a scenario characterized by extensive or diffuse contamination. Furthermore, a no flux condition was imposed at the axis of symmetry, at the vertical segment at the end of the soil layer width, and on the segments representing the depth and width of the building ($\nabla c \cdot n = 0$, black lines in Fig. 1). In Configurations 2 and 4, the no flux condition was also imposed on the segments representing the horizontal and vertical HDPE liners (illustrated as light blue lines in Fig. 1). Note that in Configuration 2 the HDPE horizontal liner (i.e., the no flux boundary condition) was assumed to overlap the HPRB for a distance of 50 cm.

To estimate vapor intrusion into the building, it was assumed that vapors enter through openings and cracks located at the interface between the floor and the walls, at a distance of 20 cm from the building perimeter (d_P) (see point P in Fig. 1). This assumption is consistent with previous vapor intrusion studies [47–50]. Note that this is a conservative assumption, as lateral bypass of vapors around the barrier is more significant at the building edges compared to the central area.

The parameters values employed for each configuration in the numerical simulations are reported in Table 1. The subsurface environment was modeled as a sandy soil, with characteristic properties selected in accordance with the U.S. EPA [51] classification and guidance for soil parameters. Porosity values for the HPRB were derived from previous studies [21,33]. The subsurface beneath the building was modeled as a homogeneous soil layer extending 50 m from the axis of symmetry (L_s) (see Fig. 1). The vapor source was assumed to originate from groundwater contaminated with trichloroethylene (TCE), which was selected as the model compound. TCE-specific parameters were obtained from the U.S. EPA database [52]. The building foundations were modeled to extend 1 m below ground level (H_b) and situated 5 m above the contaminated groundwater (H_{gw}).

The other parameters were varied through the simulations conducted for the HPRB design study for each assumed configuration (see Fig. 1). For Configurations 1 and 2, the study focused on evaluating the efficiency of the HPRB in preventing lateral bypass of contaminated vapors. In Configuration 1, which includes only the HPRB, the ratio between the barrier width and the building footprint (L_{HPRB}/L_b) varied between 1 and 2, while the barrier thickness (d_{HPRB}) was kept constant at 50 cm. In Configuration 2, where the HPRB was combined with a horizontal HDPE liner, the width of the HPRB was fixed (L_{HPRB}/L_b equal to 1.5), while the width of the HDPE liner was varied. As a result, the total ratio between the barrier width and the building footprint ($(L_{HPRB}+L_{HDPE})/L_b$) ranged from 2 to 5. In Configurations 3 and 4, a vertical barrier was added to prevent lateral contaminant bypass. In these cases, the HPRB width remained fixed with L_{HPRB}/L_b equal to 1.5, while the HPRB thickness was varied from 10 to 100 cm to investigate its influence on vapors attenuation.

In all the simulated configurations, the degradation kinetic constants of the HPRB were varied in the range of 0.1 to 10 d^{-1}, to represent different reactive materials or water contents within the barrier. This range is consistent with the values reported in the literature for the degradation of chlorinated vapors by reactive materials. For instance, Zingaretti et al. [21] reported degradation rate constants for TCE vapors in the range of 0.02–0.3 d^{-1} using ZVI powders, while Settimi et al. [33] found values between 0.6 and 5.7 d^{-1} using ZVI-based bimetallic and sulfidated materials.

Vapor intrusion mitigation assessment

The expected performances of the different HPRB configurations were assessed in terms of source-to-indoor attenuation factor (α), defined as the ratio between the indoor and the vapor source concentrations. α could be defined as the product of the subsoil attenuation factor (α_{soil}) influenced by HPRB mitigation and the attenuation factor through the building foundations (α_{ss}) that depends on the building

Table 1
Parameters employed in the numerical simulations for each HPRB configuration design. (-) indicates the absence of the specific parameter in the assumed configuration, while the parameters subjected to the design study are expressed as variables, indicating the range assumed. Configuration 1 = HPRB; Configuration 2 = HPRB+horizontal HDPE; Configuration 3 = HPRB+vertical PRB; Configuration 4 = HPRB+vertical HDPE.

Parameter	Configuration 1	Configuration 2	Configuration 3	Configuration 4
Soil Parameters (sand)				
$\theta_{e,s}$ (-)	0.375	0.375	0.375	0.375
a (m^{-1})	3.524	3.524	3.524	3.524
n (-)	3.177	3.177	3.177	3.177
m (-)	0.685	0.685	0.685	0.685
H_{gw} (m)	5	5	5	5
L_s (m)	50	50	50	50
L_b (m)	5	5	5	5
H_b (m)	1	1	1	1
d_P (m)	0.2	0.2	0.2	0.2
HPRB Parameters				
$\theta_{e,HPRB}$ (-)	0.61	0.61	0.61	0.61
$\theta_{w,HPRB}$ (-)	0.5	0.5	0.5	0.5
$\theta_{a,HPRB}$ (-)	0.11	0.11	0.11	0.11
L_{HPRB} (m)	variable (5–10)	7.5	7.5	7.5
d_{HPRB} (m)	0.5	0.5	variable (0.1–1)	variable (0.1–1)
H_{PRB} (m)	–	–	2	–
L_{HDPE} (m)	–	variable (2.5–17.5)	–	–
d_{HDPE} (m)	–	0.001	–	0.001
H_{HDPE} (m)	–	–	–	2
k (d^{-1})	variable (0.1–10)	variable (0.1–10)	variable (0.1–10)	variable (0.1–10)
Compound Parameters (TCE)				
D_a (m^2/s)	$6.67 \cdot 10^{-6}$	$6.67 \cdot 10^{-6}$	$6.67 \cdot 10^{-6}$	$6.67 \cdot 10^{-6}$
D_w (m^2/s)	$1.02 \cdot 10^{-9}$	$1.02 \cdot 10^{-9}$	$1.02 \cdot 10^{-9}$	$1.02 \cdot 10^{-9}$

characteristics and the air exchange rate [51,53]:

$$\alpha = \alpha_{soil} \cdot \alpha_{ss} \quad (7)$$

The subsoil attenuation factor (α_{soil}) was estimated with the numerical model as the ratio between the concentration at the soil to building interface (c(P)) (point P in Fig. 1) and the vapor source concentration (c_{source}):

$$\alpha_{soil} = \frac{c(P)}{c_{source}} \quad (8)$$

Instead, the attenuation factor through the building foundations (α_{ss}) was fixed at the default value of 0.03, recommended by the U.S. EPA VI Guidance [54].

To assess the mitigation efficacy of the different configurations, the modeled attenuation factors were compared with the maximum soil attenuation factor (α_{sat}) that ensures acceptable risk levels for residents in the case of vapor source concentration at saturation. Specifically, α_{sat} was estimated as the ratio between the Vapor Intrusion Screening Level, VISL (g/m^3), reported by U.S. EPA [55] and the maximum vapor concentration at saturation conditions, $c_{sat.vap}$ (g/m^3):

$$\alpha_{sat} = \frac{VISL}{c_{sat.vap} \cdot \alpha_{ss}} \quad (9)$$

$c_{sat.vap}$ (g/m^3) can be estimated as follows and represents the maximum concentration available in the vapor phase for a specific compound [56]:

$$c_{sat.vap} = S \cdot H \quad (10)$$

where S (mg/L) is the water solubility of a specific contaminant, and H is the dimensionless Henry's constant.

Furthermore, the minimum soil attenuation factor (α_{min}) required to ensure acceptable risk levels in the case of a groundwater concentration equal to the Maximum Contaminant Level, MCL (mg/L), for a specific compound [57], was calculated as follows:

$$\alpha_{MCL} = \frac{VISL}{MCL \cdot H \cdot \alpha_{ss}} \quad (11)$$

Therefore, α_{max} represents the worst scenario for vapor intrusion, thus the upper limit value to ensure with the mitigation technique. Conversely, α_{MCL} represents the attenuation to achieve for low contamination scenarios when the concentration in the source is equal to the MCL. Table 2 reports the calculated α_{sat} and α_{MCL} for different chlorinated contaminants frequently detected at contaminated sites [58].

3. Results and discussion

3.1. Model validation

The results of the developed numerical model were preliminarily compared with the output of different studies present in the literature regarding HPRBs development by modeling or experiments [21,33,36].

First, the output of the developed numerical model was compared with that of an existing 2-D transient analytical model developed by Wang et al. [36] for HPRBs. Following the setup adopted in that study, the simulation domain included two layers above the contamination source: a sandy soil layer (2.5 m wide and 1.8 m deep) overlain by a 30 cm thick HPRB extending to the ground surface. A Gaussian function was used to describe the distribution of TCE in groundwater, and the HPRB was modeled assuming a degradation rate constant of 0.14 s^{-1}. The comparison was carried out at 5 years, corresponding to steady-state conditions, by analyzing the normalized concentration profile (c/c_{source}) as a function of the vertical height (z) at two different vertical soil sections ($x = 0$ m and $x = 2$ m). Fig. 2a shows the analytical results from Wang et al. [36] as indicators and the numerical results from this study as continuous lines. The same input parameters were used in both models (see Table 1). The comparison demonstrates a strong agreement between the models, with a high correlation coefficient ($R^2 = 0.99$).

Then, the results of the developed model were compared with the output of the 1-D steady-state analytical solution reported by Zingaretti et al. [21] for describing the attenuation expected in an HPRB as a function of the first-order degradation kinetics. The developed model was adapted to the conditions assumed by Zingaretti et al. [21], i.e., simulating an HPRB with different thicknesses in the range 0.25–1 m, with a porosity ($\theta_{e,HPRB}$) of 0.5 and an air filled porosity ($\theta_{a,HPRB}$) of 0.15. To derive the analytical solution, Zingaretti et al. [21] imposed a fixed initial concentration entering the barrier and a no flux boundary condition at an infinite distance from the end of the HPRB. To replicate the latter condition in the developed numerical model, a layer of 100 m was built in the geometry to impose the no flux boundary condition. Fig. 2b shows the analytical results from Zingaretti et al. [21] as indicators and the numerical results from this study as continuous lines, showing excellent correlation in all the simulated scenarios ($R^2 = 0.99$).

Finally, the results of the developed model were compared with the experimental data obtained by Settimi et al. [33] who performed TCE vapor degradation column tests using a reactive layer made of sulfidated ZVI-Ni bimetal Such results are reported in Fig. 2c as indicators of the average concentration values detected at different test times, ranging from 4 to 25 d, in which steady-state conditions were achieved [33], with error bars indicating the standard deviation among the values obtained in time. Also in this case, the numerical model was adapted to match the experimental conditions applied by Settimi et al. [33] by creating a geometry in the model builder that replicated the column setup, constituted by a 10 cm glass beads/sand layer, a 5 cm of HPRB and a final 10 cm of glass beads. The effective porosity and diffusion coefficient in the porous media were the same reported in Table 1 and the degradation constant relative to the sulfidated ZVI-Ni bimetal was posed equal to 0.6 d^{-1}, i.e., derived from the column experiments conducted by Settimi et al. [33]. Boundary conditions were defined by imposing a fixed concentration entering the first glass beads layer ($z = 0$) and a concentration equal to zero outgoing the column ($z = 30$ cm).

Table 2
Parameters selected for evaluating the minimum and maximum soil attenuation factors using the U.S. EPA limit values for MCL [57] and VISL [55] for different chlorinated compounds. (-) was reported when no attenuation was required ($\alpha > 1$).

Compound	S (mg/L)	H (-)	$c_{sat,vap}$ (g/m^3)	MCL (mg/L)	VISL (g/m^3)	α_{MCL} (-)	α_{sat} (-)
1,2-Dichloroethane	8600	0.048	415	0.005	$1.08 \cdot 10^{-7}$	$1.49 \cdot 10^{-2}$	$8.68 \cdot 10^{-9}$
1,1,1-Trichloroethane	1290	0.703	907	0.2	$5.21 \cdot 10^{-4}$	$1.23 \cdot 10^{-1}$	$1.91 \cdot 10^{-5}$
1,1,2-Trichloroethane	4590	0.034	155	0.005	$1.75 \cdot 10^{-7}$	$3.46 \cdot 10^{-2}$	$3.77 \cdot 10^{-8}$
Vinyl Chloride	8800	1.100	9680	0.002	$1.68 \cdot 10^{-7}$	$2.55 \cdot 10^{-3}$	$5.79 \cdot 10^{-10}$
1,1-Dichloroethylene	2420	1.067	2582	0.007	$4.13 \cdot 10^{-7}$	$1.84 \cdot 10^{-3}$	$5.33 \cdot 10^{-9}$
cis-1,2-Dichloroethylene	6410	0.167	1069	0.07	$4.17 \cdot 10^{-6}$	$1.19 \cdot 10^{-2}$	$1.30 \cdot 10^{-7}$
Trichloroethylene	1280	0.403	515	0.005	$4.78 \cdot 10^{-7}$	$7.91 \cdot 10^{-3}$	$3.09 \cdot 10^{-8}$
Tetrachloroethylene	206	0.724	149	0.005	$1.08 \cdot 10^{-5}$	$9.95 \cdot 10^{-2}$	$2.42 \cdot 10^{-6}$
Carbon tetrachloride	793	1.128	895	0.005	$4.68 \cdot 10^{-7}$	$2.77 \cdot 10^{-3}$	$1.74 \cdot 10^{-8}$
Dichloromethane	13000	0.133	1727	0.005	$6.26 \cdot 10^{-5}$	–	$1.21 \cdot 10^{-6}$
Chlorobenzene	498	0.127	63	0.1	$5.21 \cdot 10^{-6}$	$1.37 \cdot 10^{-2}$	$2.74 \cdot 10^{-6}$

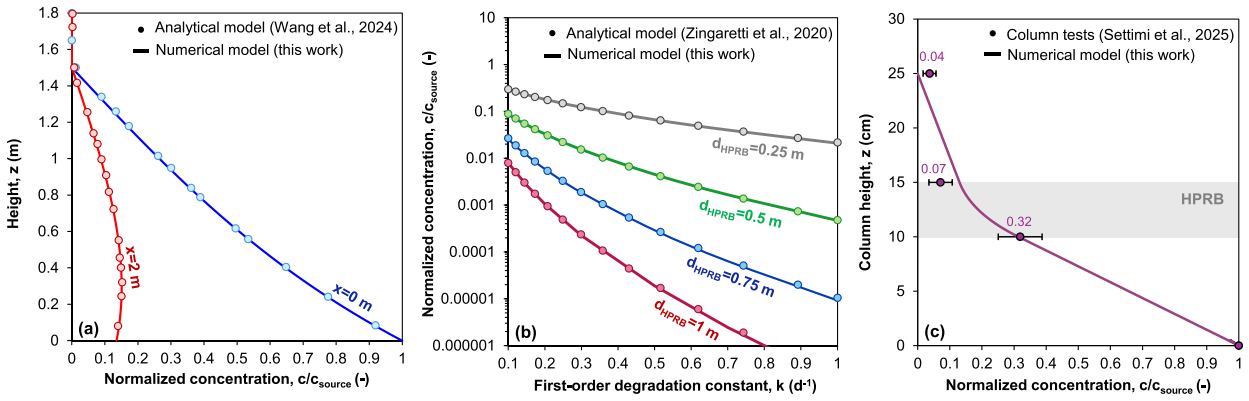

Fig. 2. Comparison between the output of the numerical model developed in this work (continuous lines) and the results of different studies: (a) Analytical model [36] (indicators) in terms of normalized concentration as a function of the vertical height from the source, (b) Analytical model [21] (indicators) in terms of first-order degradation constant in the vapor phase as a function of normalized concentration, (c) experimental data derived from column tests conducted in the time range of 4–25 d [33] (indicators) in terms of column height.

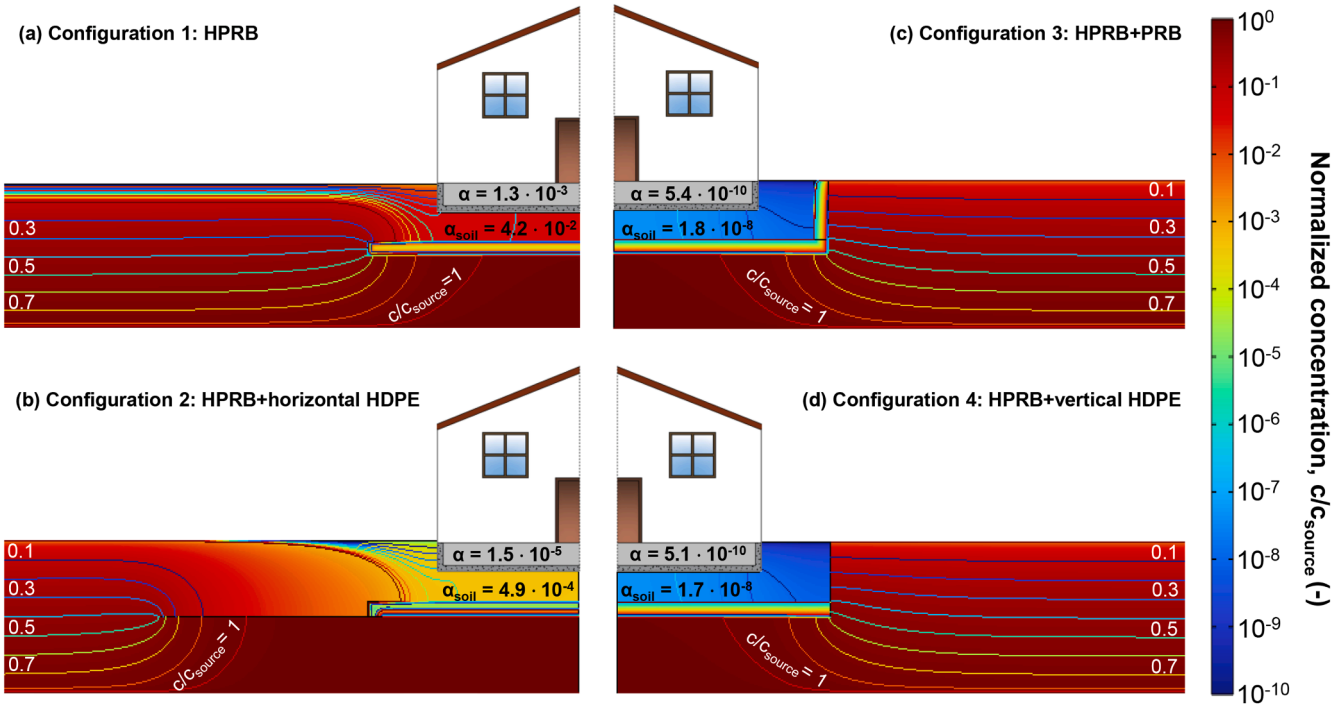

Fig. 3. Normalized soil gas concentrations (c/c_{source}) for each HPRB configuration. In each subfigure the soil attenuation factor (α_{soil}) and source-to-indoor attenuation factor (α) are also shown. In these simulations the degradation constant (k) in the HPRB was set equal to 1 d^{-1} and the barrier thickness (d_{HPRB}) equal to 50 cm. For Configurations 1, 3, and 4, the ratio L_{HPRB}/L_b was set to 1.5 while for Configuration 2, the combined length of the HPRB and HDPE liner relative to the building $(L_{HPRB}+L_{HDPE})/L_b$ was set to 3.

Fig. 2c reports the output of the developed numerical model as continuous line, showing good correlation with the experimental results (R^2 = 0.99).

The comparison between the output of the developed numerical model and the different modeling and experimental results supports the validity of the numerical solution developed in this work.

3.2. Role of lateral bypass of vapors beyond the barrier

Fig. 3 shows an example of the 2-D distribution of the normalized soil gas concentration (c/c_{source}) and the corresponding soil attenuation factor (α_{soil}) and source-to-indoor attenuation factor (α) obtained for each HPRB configuration simulated with the numerical model. Namely, these results refer to the case where the degradation rate constant (k) in the HPRB was assumed equal to 1 d^{-1} and the barrier thickness (d_{HPRB}) to 50 cm. For Configurations 1, 3, and 4, the ratio L_{HPRB}/L_b was set to 1.5 while for Configuration 2, the combined width of the HPRB and HDPE liner relative to the building, $(L_{HPRB}+L_{HDPE})/L_b$, was set to 3. The other input parameters are reported in Table 1.

It can be observed from Fig. 3 that lateral bypass of vapors beyond the barrier is a critical issue in Configurations 1 and 2. In Configuration 1 (Fig. 3a), the sole presence of a horizontal reactive layer is not effective to mitigate vapors, as lateral diffusion of vapors in the soil beyond the barrier is dominant. In this configuration, indeed, the estimated value of the soil attenuation factor under the foundations was approximately 10^{-2} that is ineffective for many contaminants reported in Table 2. For instance, for a groundwater contaminated by Vinyl Chloride, 1,1-Dichloroethylene or Trichloroethylene the soil attenuation factors that

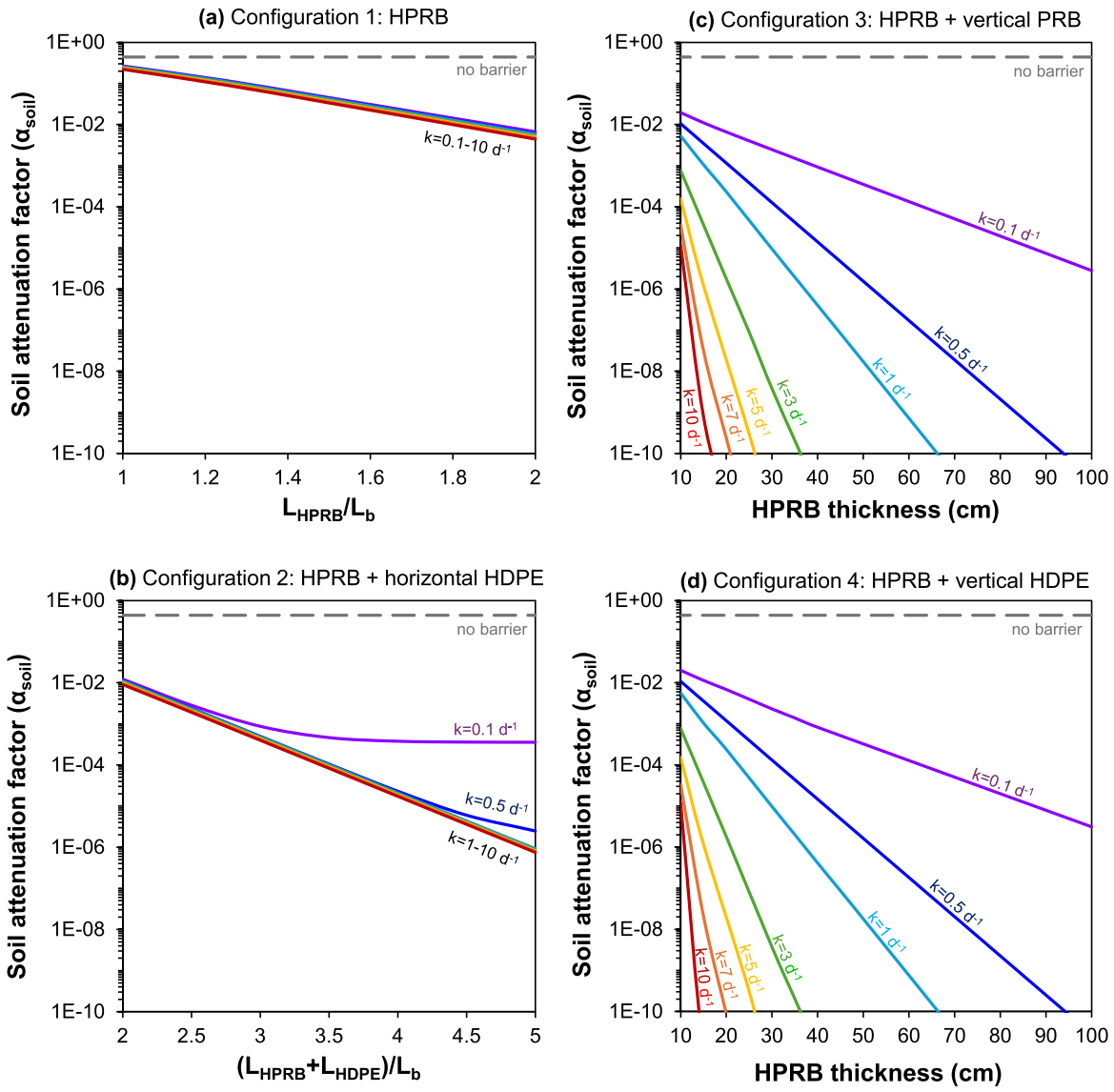

Fig. 4. Soil attenuation factors beneath the foundations as a function of the investigated design parameters for different degradation rate constants (0.1–10 d^{-1}). The baseline soil attenuation factor without any barrier is also shown for comparison. Subfigures (a) and (b) correspond to Configurations 1 and 2, respectively, where the variation in the soil attenuation factor was analyzed by changing the ratio between the barrier and crawlspace widths (L_{HPRB}/L_b in Configuration 1 and $(L_{HPRB}+L_{HDPE})/L_b$ in Configuration 2). Subfigures (c) and (d) illustrate Configurations 3 and 4, respectively, where the analysis focused on the effects of HPRB thickness (d_{HPRB}).

ensure acceptable risks in the case of contamination equal to MCL (α_{MCL}) must be in the order of 10^{-3} (see Table 2). It is worth noting that Wang et al. [36], who modeled an infinitely wide horizontal barrier and neglected lateral bypass, reported attenuation factors of 10^{-8} for a 50 cm thick layer. Thus, this comparison highlights the importance of accounting for the barrier width to accurately estimate the expected attenuation factor.

Configuration 2 (Fig. 3b), which includes an HDPE horizontal liner, increases the lateral diffusion length of vapors beyond the barriers leading to soil attenuation factors below the buildings foundations in the order of 10^{-4} that make this option feasible in the case low-contamination scenarios (i.e., slightly above MCL). Conversely, Configurations 3 and 4 (Fig. 3c and Fig. 3d) which incorporate a vertical reactive layer, achieve much greater mitigation ($\alpha_{soil} \approx 10^{-8}$), comparable to the idealized scenario of infinitely wide barrier simulated in Wang et al. [36], and demonstrate the effectiveness of including vertical components in HPRB design.

3.3. Nomographs for HPRB design

To assess the applicability of each HPRB configuration, a series of simulations were performed exploring different HPRB geometries (in terms of lateral extent and thickness) and reactive materials (characterized by different degradation rate constants). Fig. 4 summarizes the resulting soil attenuation factors beneath the foundations, reported as a function of these parameters. The baseline soil attenuation factor without any barrier is also shown for comparison.

For Configurations 1 and 2 (Fig. 4a and Fig. 4b), which include only horizontal layers, the analysis focused on the lateral extent of the barrier to assess its role in limiting vapor lateral bypass. In Configurations 3 and 4 (Fig. 4c and Fig. 4d), which also include vertical layers surrounding the building, the lateral extent was fixed ($L_{HPRB}/L_b = 1.5$), and the influence of barrier thickness was evaluated. The other input parameters are reported in Table 1.

In Fig. 4a (Configuration 1), where only a horizontal reactive layer is placed beneath the building, results show that the attenuation factor is

mainly controlled by the L_{HPRB}/L_b ratio, with negligible impact from the degradation constant. Even with large lateral extents, attenuation remains low (in the order of 10^{-2}), indicating poor effectiveness in reducing vapor intrusion and limiting this design to sites with very low contamination levels (see Table 2).

Fig. 4b (Configuration 2) explores the combined lateral extent of the reactive and HDPE liner. Here, the degradation kinetics have a stronger influence, but as degradation rate increases, attenuation is again driven primarily by lateral extension. Higher attenuation (10^{-6} to 10^{-4}) can be achieved with sufficient barrier length, making this configuration suitable for higher contamination levels. However, practical implementation may be constrained by the need for substantial subsurface coverage. For example, achieving a soil attenuation factor of 10^{-6} may require a combined barrier width of 50 m for a building footprint of 10 m (assuming $(L_{HPRB} + L_{HDPE})/L_b = 5$), which could be challenging to install.

Fig. 4c and Fig. 4d (Configurations 3 and 4) present scenarios with vertical layers surrounding the building, combined with an HPRB. In these cases, lateral extension plays a minor role, and the focus shifts to the effects of barrier thickness and reactivity. Both parameters significantly influence the attenuation factor, which can vary by orders of magnitude depending on the degradation constant. These configurations yield high attenuation (10^{-10} to 10^{-6}), making them suitable for sites with elevated contamination (see Table 2). Moreover, their implementation may be more practical due to reduced excavation needs and the absence of extensive horizontal HDPE liners, making them promising solutions for chlorinated vapor mitigation.

It should be highlighted that the installation of both horizontal and vertical barriers near existing buildings may present technical challenges. In particular, soil excavation and the placement of reactive materials must be carried out with great care to avoid any risk of structural destabilization. In contrast, when the proposed technique is applied in the context of brownfield redevelopment projects (e.g., for new residential areas), potential issues such as soil subsidence and impacts on future foundations can be more accurately monitored and managed.

3.4. Influence of barrier thickness

Designing a VI mitigation system based on Configurations 3 and 4 allows for a broad range of achievable soil attenuation factors. As shown in Fig. 4c and Fig. 4d, both configurations ensure significantly higher performance compared to those relying only on horizontal layers (Fig. 4a and Fig. 4b). Between the two, Configuration 3, featuring a vertical reactive layer, offers the added benefit of allowing vapor to pass through rather than accumulate in the subsurface.

With Configuration 3, once the properties of the reactive material, particularly the degradation constant and the moisture content, are known, the required HPRB thickness can be tailored to meet project-specific attenuation targets. Fig. 5 illustrates how barrier thickness influences soil and indoor attenuation factors in the case of a degradation constant (k) of 1 d^{-1}. The normalized soil gas concentration distribution (c/c_{source}) is displayed on a logarithmic scale to highlight differences across design scenarios.

These results confirm that a wide range of attenuation levels can be achieved simply by adjusting the barrier thickness. This trend is consistent with previous 2-D modeling studies [36–38], which demonstrated improved performance with increasing barrier thickness. Notably, effective soil attenuation (α_{soil} in the order of 10^{-4} to 10^{-3}) can be obtained even with relatively thin barriers (10–20 cm, see Fig. 5a and Fig. 5b), comparable to the performance of Configuration 2 with $(L_{HPRB} + L_{HDPE})/L_b = 3$ and a 50 cm thick barrier.

Beyond its performance, this design also simplifies installation and significantly reduces the quantity of reactive material required, leading to lower construction and maintenance costs. Additionally, as shown in Fig. 5c and Fig. 5d, this configuration is capable of reaching high attenuation, meeting the upper limit of attenuation factors required in the case of saturation conditions in the source zone (i.e., α_{sat} values reported in Table 2).

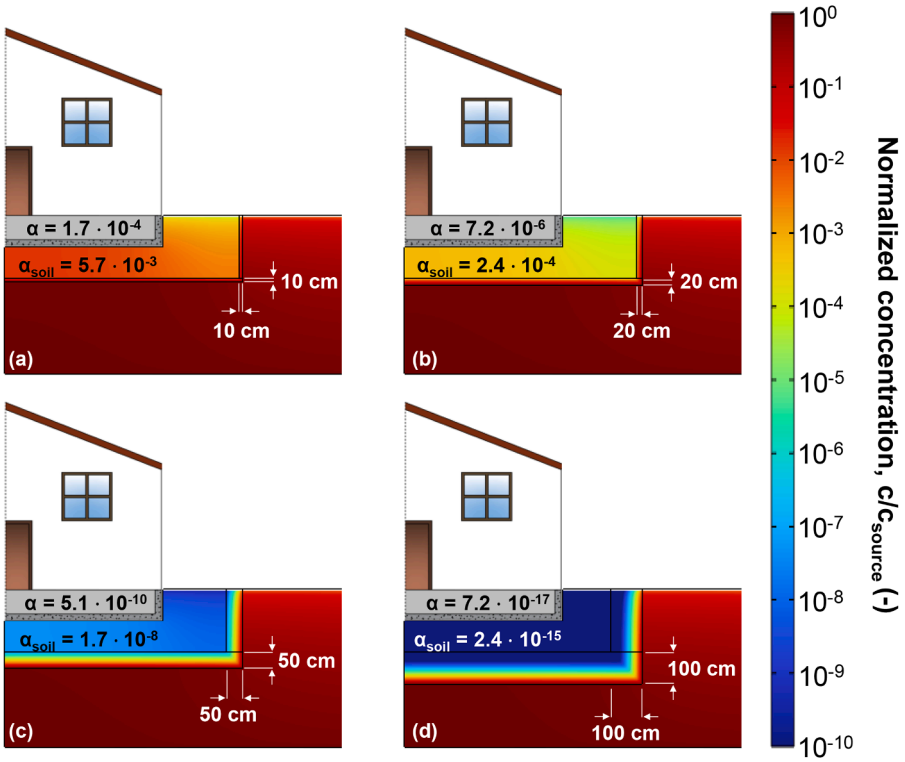

Fig. 5. Normalized soil gas concentrations (c/c_{source}) for for varying barrier thicknesses in Configuration 3 (HPRB + PRB). In each subfigure the soil attenuation factor (α_{soil}) and source-to-indoor attenuation factor (α) are also shown. In these simulations the degradation constant (k) in the HPRB was set equal to 1 d^{-1}.

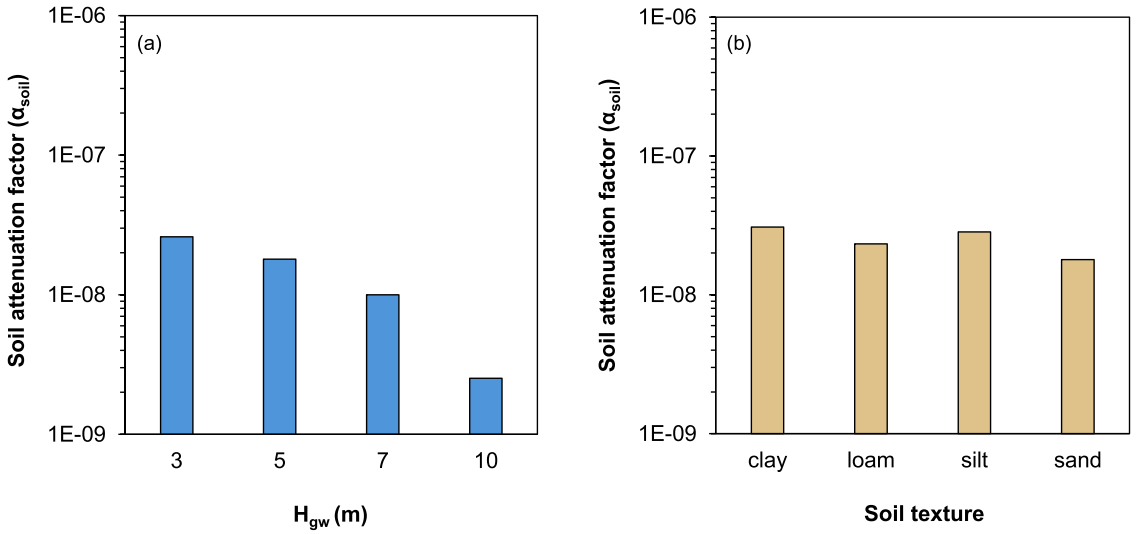

Fig. 6. Soil attenuation factor calculated with the numerical model for Configuration 3 (HPRB + PRB) as a function of (a) the groundwater table depth (H_{gw}) and (b) the soil texture. Simulations were conducted assuming a degradation rate constant of 1 d^{-1} and an HPRB thickness of 50 cm.

3.5. Influence of subsurface conditions

A sensitivity analysis was carried out to evaluate the influence of subsurface conditions on the resulting soil attenuation factor. The analysis focused on Configuration 3, identified as the most effective and practical approach for vapor intrusion mitigation. Specifically, the effects of groundwater table depth (H_{gw}) and soil texture within the unsaturated zone were examined (Fig. 6). Simulations were conducted assuming a degradation rate constant of 1 d^{-1} and an HPRB thickness of 50 cm.

Fig. 6a presents the variation in the soil attenuation factor with groundwater depths ranging from 3 to 10 m A decreasing trend in the attenuation factor (i.e., increased attenuation performance) is observed with increasing groundwater depth, attributed to the greater separation between the vapor source and the building. Notably, for lower depths of 3 and 5 m, attenuation values remain nearly constant, indicating the robustness of Configuration 3 even under more challenging shallow contamination scenarios.

Soil type can influence the vertical moisture profile above the water table, consequently affecting vapor diffusion in the unsaturated zone beneath the reactive barrier. To assess how soil characteristics might impact the results previously obtained for sandy soil, simulations were conducted for Configuration 3 assuming four different soil types (sand, loam, silt, and clay). For each soil, vertical moisture profiles were estimated using the Van Genuchten empirical parameters and soil properties reported by U.S. EPA [43]. The results of these simulations, expressed as attenuation factors within the soil, are shown in Fig. 6b. It can be noticed that the expected attenuation factors beneath the foundations in the presence of a reactive barrier are only minimally affected by the type of natural soil present. Slightly higher attenuation factors are expected for less permeable soils (e.g., clay), where, as demonstrated in previous studies (e. g., [50,59]), vapor fluxes in the subsurface tend to be lower due to reduced diffusion, leading to greater accumulation compared to more permeable soils (e.g., sand).

Similar outcomes were found by Wang et al. [36], which observed better performances of the HPRB by increasing the source depth and overall negligible influence of the soil type by changing its effective diffusivity.

4. Conclusions

The results of the developed numerical model demonstrate that only a horizontal barrier composed of reactive material (Configuration 1) is insufficient to ensure adequate vapor attenuation at sites with contaminant concentrations exceeding regulatory limits, primarily due to lateral bypass of vapors. Even when using highly reactive filling materials, this configuration achieves attenuation factors in the order of 10^{-3}, which may be acceptable solely for sites with contamination levels in groundwater slightly above the Maximum Contaminant Levels (MCLs). The addition of a horizontal HDPE liner (Configuration 2) enhances performance by reducing the lateral bypass effect. However, this improvement requires extensive HDPE coverage beneath the building footprint to guarantee elevated attenuation levels, resulting in substantial excavation volumes and technical implementation challenges. These outcomes suggest that its application is more suitable for low or moderate contamination scenarios, offering a balanced solution in terms of both cost-efficiency and mitigation performance.

Configurations combining a horizontal permeable reactive barrier with a vertical reactive layer (Configuration 3) or a vertical HDPE liner (Configuration 4) proved to be the most effective. These configurations achieved attenuation factors in the order of 10^{-10}, even under saturated groundwater conditions, thus ensuring acceptable indoor risk across a wide range of contamination scenarios. Furthermore, high attenuation levels can be reached with reduced material thickness (10–20 cm) and moderate reactivity, supporting the cost-effectiveness and technical feasibility of these designs, thereby confirming their viability even for sites with elevated groundwater contamination levels.

It is worth noting that the results presented in this study were obtained under simplified modeling assumptions, such as steady-state conditions and homogeneous soil properties, which were adopted to estimate the performance of the HPRB system. These assumptions imply the exclusion of potentially relevant transient phenomena (e.g., changes in saturation due to rainfall events) and subsurface heterogeneity, which may influence vapor transport dynamics [18,60,61]. While these simplifications are appropriate for the conceptual design stage and for understanding the general system behavior, in the case of complex site-specific conditions or for detailed barrier design, the use of more advanced numerical models (e.g., 3-D transient models accounting for heterogeneity and dynamic boundary conditions) could be recommended. Additionally, the integration of pilot-scale on-site experiments could further support model validation and enhance confidence in performance predictions.

Nevertheless, the results of this study support the general applicability of horizontal permeable reactive barriers, particularly when

integrated with vertical layers, as a passive mitigation strategy for managing chlorinated vapor intrusion risks.

Nomenclature

Symbol	Parameter	Unit
a	Van Genuchten parameter	[L^{-1}]
c	Contaminant vapor concentration	[M/L^3]
$c_{sat.vap}$	Contaminant saturation concentration in the vapor phase	[M/L^3]
c_{source}	Contaminant source vapor concentration	[M/L^3]
D_s	Effective diffusion coefficient in the soil layer	[L^2/T]
D_{HPRB}	Effective diffusion coefficient in the reactive layer	[L^2/T]
D_a	Contaminant air diffusion coefficient	[L^2/T]
D_w	Contaminant water diffusion coefficient	[L^2/T]
d_{HPRB}	Reactive layers thickness	[L]
d_{HDPE}	HDPE liner thickness	[L]
d_P	Foundation walls thickness	[L]
H	Contaminant dimensionless Henry's constant	[-]
H_b	Building foundations depth from the ground surface	[L]
H_{gw}	Groundwater depth from ground surface	[L]
H_{HDPE}	Vertical HDPE liner depth	[L]
H_{PRB}	Vertical reactive layer depth	[L]
k	Degradation constant in the vapor phase	[T^{-1}]
k_1	First-order kinetic degradation constant in the water phase	[T^{-1}]
L_{HDPE}	Horizontal HDPE liner width	[L]
L_{HPRB}	Horizontal reactive layer width	[L]
L_b	Building width	[L]
L_s	Soil layer width	[L]
m	Van Genuchten parameter	[-]
n	Van Genuchten parameter	[-]
MCL	Maximum Contaminant Level	[M/L^3]
S	Contaminant solubility in water	[M/L^3]
VISL	Vapor Intrusion Screening Level	[M/L^3]
α	Source-to-indoor attenuation factor	[-]
α_{MCL}	Attenuation factor imposing a source concentration equal to the MCL	[-]
α_{sat}	Attenuation factor imposing a source concentration equal to the saturation	[-]
α_{soil}	Soil attenuation factor	[-]
α_{ss}	Attenuation factor in the foundations	[-]
θ_a	Layer volumetric gas content	[-]
θ_e	Layer effective porosity	[-]
θ_r	Layer residual water content	[-]
θ_s	Layer saturated water content	[-]
θ_w	Layer volumetric water content	[-]

CRediT authorship contribution statement

Nicolò Tonolo: Writing – original draft, Methodology, Investigation, Formal analysis, Data curation, Conceptualization. **Clarissa Settimi:** Writing – original draft, Methodology, Investigation, Formal analysis, Data curation, Conceptualization. **Daniela Zingaretti:** Writing – review & editing, Supervision, Methodology. **Renato Baciocchi:** Supervision, Resources. **Iason Verginelli:** Writing – review & editing, Supervision, Methodology, Conceptualization.

Declaration of competing interest

The authors declare that they have no known competing financial interests or personal relationships that could have appeared to influence the work reported in this paper.

Data availability

Data will be made available on request.

References

[1] B. Huang, C. Lei, C. Wei, G. Zeng, Chlorinated volatile organic compounds (Cl-VOCs) in environment — Sources, potential human health impacts, and current remediation technologies, Environ. Int. 71 (2014) 118–138, https://doi.org/10.1016/j.envint.2014.06.013.

[2] W. Li, W. Zhang, J. Dong, X. Liang, C. Sun, Groundwater chlorinated solvent plumes remediation from the past to the future: a scientometric and visualization analysis, Environ. Sci. Pollut. Res. 31 (2024) 17033–17051, https://doi.org/10.1007/s11356-024-32080-z.

[3] P.L. McCarty, in: H.F. Stroo, C.H. Ward (Eds.), Groundwater Contamination by Chlorinated Solvents: History, Remediation Technologies and Strategies, Situ Remediat. Chlorinated Solvent Plumes, Springer, New York, New York, NY, 2010, pp. 1–28, https://doi.org/10.1007/978-1-4419-1401-9_1.

[4] J. Koenig, M. Lee, M. Manefield, Aliphatic organochlorine degradation in subsurface environments, Rev. Environ. Sci. Biotechnol. 14 (2015) 49–71, https://doi.org/10.1007/s11157-014-9345-3.

[5] M.J. Moran, J.S. Zogorski, P.J. Squillace, Chlorinated solvents in groundwater of the United States, Environ. Sci. Technol. 41 (2007) 74–81, https://doi.org/10.1021/es061553y.

[6] U.S. AFERP, United States Air Force Environmental Restoration Program. Remediation of Chlorinated Solvent Contamination on Industrial and Airfield Sites. https://www.clu-in.org/download/contaminantfocus/dnapl/treatment_technologies/remediation_of_chlorinated_dnapl_afceeaf_chlor.pdf (accessed on March 2025), (2000).

[7] A. Azzellino, L. Colombo, S. Lombi, V. Marchesi, A. Piana, M. Andrea, L. Alberti, Groundwater diffuse pollution in functional urban areas: the need to define anthropogenic diffuse pollution background levels, Sci. Total Environ. 656 (2019) 1207–1222, https://doi.org/10.1016/j.scitotenv.2018.11.416.

[8] A. Guleria, P.K. Gupta, S. Chakma, B.K. Yadav, Unraveling the fate and transport of DNAPLs in heterogeneous aquifer systems—A critical review and bibliometric analysis, Sustainability 15 (2023) 8214, https://doi.org/10.3390/su15108214.

[9] L. Semprini, In situ bioremediation of chlorinated solvents, Environ. Health Perspect. 103 (1995).

[10] O. Al-Hashimi, K. Hashim, E. Loffill, T. Marolt Čebašek, I. Nakouti, A.A.H. Faisal, N. Al-Ansari, A comprehensive review for Groundwater contamination and remediation: occurrence, migration and adsorption modelling, Molecules 26 (2021) 5913, https://doi.org/10.3390/molecules26195913.

[11] M.O. Rivett, G.P. Wealthall, R.A. Dearden, T.A. McAlary, Review of unsaturated-zone transport and attenuation of volatile organic compound (VOC) plumes leached from shallow source zones, J. Contam. Hydrol. 123 (2011) 130–156, https://doi.org/10.1016/j.jconhyd.2010.12.013.

[12] U.S. E.P.A., In situ thermal treatment of chlorinated solvents: fundamentals and field applications. https://www.epa.gov/remedytech/situ-thermal-treatment-chlorinated-solvents-fundamentals-and-field-applications (accessed on September 2024)., (2004).

[13] B. Eklund, C. Regan, R. Rago, L. Beckley, Overview of State approaches to vapor intrusion: 2023 update, Groundw. Monit. Remediat. 44 (2024) 76–93, https://doi.org/10.1111/gwmr.12627.

[14] J. Ma, T. McHugh, L. Beckley, M. Lahvis, G. DeVaull, L. Jiang, Vapor intrusion investigations and decision-making: a critical review, Environ. Sci. Technol. 54 (2020) 7050–7069, https://doi.org/10.1021/acs.est.0c00225.

[15] T. McHugh, P. Loll, B. Eklund, Recent advances in vapor intrusion site investigations, J. Environ. Manage. 204 (2017) 783–792, https://doi.org/10.1016/j.jenvman.2017.02.015.

[16] J.S. Rios Mora, B. Collignan, T. Diallo, M. Abadie, K. Limam, Numerical analysis of vapor intrusion from the ground into buildings in the presence of lateral sources of pollution, Build. Environ. 207 (2022) 108397, https://doi.org/10.1016/j.buildenv.2021.108397.

[17] A. Unnithan, D.N. Bekele, S. Chadalavada, R. Naidu, Insights into vapour intrusion phenomena: current outlook and preferential pathway scenario, Sci. Total Environ. 796 (2021) 148885, https://doi.org/10.1016/j.scitotenv.2021.148885.

[18] I. Verginelli, Y. Yao, A review of recent vapor intrusion modeling work, Groundw. Monit. Remediat. 41 (2021) 138–144, https://doi.org/10.1111/gwmr.12455.

[19] J.S. Rios Mora, T. Diallo, B. Collignan, M. Abadie, K. Limam, Building modeling approach for IAQ assessment: influence of the main drivers of vapor intrusion from the subsurface, Build. Environ. 245 (2023) 110825, https://doi.org/10.1016/j.buildenv.2023.110825.

[20] ITRC, remediation and institutional controls as vapor intrusion mitigation. https://vim-1.itrcweb.org/wp-content/uploads/2020/12/1-Fact-Sheet-Remediaton-FS-ForWebDev-2020-11.pdf (accessed on January 2025), (2020).

[21] D. Zingaretti, I. Verginelli, I. Luisetto, R. Baciocchi, Horizontal permeable reactive barriers with zero-valent iron for preventing upward diffusion of chlorinated solvent vapors in the unsaturated zone, J. Contam. Hydrol. 234 (2020) 103687, https://doi.org/10.1016/j.jconhyd.2020.103687.

[22] Itrc, Vapor intrusion pathway: a practical guideline. https://semspub.epa.gov/work/01/533755.pdf, (2007).

[23] T.A. McAlary, Subslab depressurization versus Subslab ventilation: insights from recent research, Groundw. Monit. Remediat. 41 (2021) 132–137, https://doi.org/10.1111/gwmr.12443.

[24] U.S. EPA, indoor air vapor intrusion mitigation approaches. https://citeseerx.ist.psu.edu/document?repid=rep1&type=pdf&doi=27db42820db00c5909db291c041d5f01eaaedf8c, (2008).

[25] N. Ding, C. Hou, H. Li, H. Chen, P. Dahlen, P.C. Johnson, Y. Yao, Y. Guo, Impact of drainage pipe vapor intrusion pathways on sub-slab depressurization system

mitigation performance, J. Hazard. Mater. 480 (2024) 136277, https://doi.org/10.1016/j.jhazmat.2024.136277.
[26] C. Lutes, L. Stewart, R. Truesdale, J. De Loera, J.H. Zimmerman, B. Schumacher, Cost comparison of soil vapor extraction and subslab depressurization for vapor intrusion mitigation, Groundw. Monit. Remediat. 42 (2022) 43–53, https://doi.org/10.1111/gwmr.12510.
[27] M.G. Mahmoodlu, S.M. Hassanizadeh, N. Hartog, A. Raoof, M.Th.Van Genuchten, Evaluation of a horizontal permeable reactive barrier for preventing upward diffusion of volatile organic compounds through the unsaturated zone, J. Environ. Manage. 163 (2015) 204–213, https://doi.org/10.1016/j.jenvman.2015.08.025.
[28] I. Verginelli, O. Capobianco, N. Hartog, R. Baciocchi, Analytical model for the design of in situ horizontal permeable reactive barriers (HPRBs) for the mitigation of chlorinated solvent vapors in the unsaturated zone, J. Contam. Hydrol. 197 (2017) 50–61, https://doi.org/10.1016/j.jconhyd.2016.12.010.
[29] M.G. Mahmoodlu, S.M. Hassanizadeh, N. Hartog, A. Raoof, Oxidation of trichloroethylene, toluene, and ethanol vapors by a partially saturated permeable reactive barrier, J. Contam. Hydrol. 164 (2014) 193–208, https://doi.org/10.1016/j.jconhyd.2014.05.013.
[30] C. Settimi, D. Zingaretti, S. Sanna, I. Verginelli, I. Luisetto, A. Tebano, R. Baciocchi, Synthesis and characterization of zero-valent Fe-Cu and Fe-Ni bimetals for the dehalogenation of trichloroethylene vapors, Sustainability 14 (2022) 7760, https://doi.org/10.3390/su14137760.
[31] D. Zingaretti, I. Verginelli, R. Baciocchi, Dehalogenation of trichloroethylene vapors by partially saturated zero-valent iron, Sci. Total Environ. 647 (2019) 682–689, https://doi.org/10.1016/j.scitotenv.2018.08.011.
[32] C. Settimi, D. Zingaretti, I. Verginelli, R. Baciocchi, Degradation of trichloroethylene vapors by micrometric zero-valent Fe Cu and Fe Ni bimetals under partially saturated conditions, J. Contam. Hydrol. 257 (2023) 104204, https://doi.org/10.1016/j.jconhyd.2023.104204.
[33] C. Settimi, D. Zingaretti, I. Verginelli, R. Baciocchi, Sulfidated zero-valent iron bimetals for passive remediation of chlorinated vapors in the subsurface, Environ. Pollut. (2025) 126202, https://doi.org/10.1016/j.envpol.2025.126202.
[34] T.J. Campbell, D.R. Burris, A.L. Roberts, J.R. Wells, Trichloroethylene and tetrachloroethylene reduction in a metallic iron–water-vapor batch system, Environ. Toxicol. Chem. 16 (1997) 625–630, https://doi.org/10.1002/etc.5620160404.
[35] S. Uludag-Demirer, A.R. Bowers, Gas phase reduction of chlorinated VOCS by zero valent iron, J. Environ. Sci. Health Part A 36 (2001) 1535–1547, https://doi.org/10.1081/ESE-100105729.
[36] S. Wang, L. Song, H. He, W. Zhang, A two-dimensional analytical model for volatile organic compound diffusion through the unsaturated soil and horizontal permeable reactive barriers, Water. Air. Soil Pollut. 235 (2024) 414, https://doi.org/10.1007/s11270-024-07211-4.
[37] Z.-W. Zhu, S.-J. Feng, Q.-T. Zheng, H.-X. Chen, H. Wei, Analytical model for the mitigation of VOC vapor with horizontal permeable reactive barrier in the contaminated site considering non-uniform source, Sci. Total Environ. 948 (2024) 174746, https://doi.org/10.1016/j.scitotenv.2024.174746.
[38] Y. Shi, H. Xie, M. Zhang, M. Ci, A transient analytical model for VOC transport through the PRB and cover layer system, J. Hydrol. 653 (2025) 132784, https://doi.org/10.1016/j.jhydrol.2025.132784.
[39] J. Massmann, D.F. Farrier, Effects of atmospheric pressures on gas transport in the vadose zone, Water Resour. Res. 28 (1992) 777–791, https://doi.org/10.1029/91WR02766.
[40] Y. Yao, R. Shen, K.G. Pennell, E.M. Suuberg, A review of vapor intrusion models, Environ. Sci. Technol. 47 (2013) 2457–2470, https://doi.org/10.1021/es302714g.
[41] R.J. Millington, J.P. Quirk, Permeability of porous solids, Trans. Faraday Soc. 57 (1961) 1200, https://doi.org/10.1039/tf9615701200.
[42] M.Th. Van Genuchten, A closed-form equation for predicting the hydraulic conductivity of unsaturated soils, Soil Sci. Soc. Am. J. 44 (1980) 892–898, https://doi.org/10.2136/sssaj1980.03615995004400050002x.
[43] U.S. EPA, user's guide for evaluating subsurface vapor intrusion into buildings. https://www.epa.gov/sites/default/files/2015-11/documents/2004_0222_3phase_users_guide.pdf (accessed on September 2024), (2004).
[44] I. Verginelli, R. Baciocchi, Modeling of vapor intrusion from hydrocarbon-contaminated sources accounting for aerobic and anaerobic biodegradation, J. Contam. Hydrol. 126 (2011) 167–180, https://doi.org/10.1016/j.jconhyd.2011.08.010.
[45] X. Liu, M. Wu, J. Zhao, Removal of trichloroethylene from water by bimetallic Ni/Fe nanoparticles, Water 14 (2022) 1616, https://doi.org/10.3390/w14101616.
[46] A. Venkateshaiah, D. Silvestri, S. Wacławek, R.K. Ramakrishnan, K. Krawczyk, P. Saravanan, M. Pawlyta, V.V.T. Padil, M. Černík, D.D. Dionysiou, A comparative study of the degradation efficiency of chlorinated organic compounds by bimetallic zero-valent iron nanoparticles, Environ. Sci. Water Res. Technol. 8 (2022) 162–172, https://doi.org/10.1039/d1ew00791b.
[47] L.D.V. Abreu, P.C. Johnson, Simulating the effect of aerobic biodegradation on soil vapor intrusion into buildings: influence of degradation rate, source concentration, and depth, Environ. Sci. Technol. 40 (2006) 2304–2315, https://doi.org/10.1021/es051335p.
[48] L.D.V. Abreu, P.C. Johnson, Effect of vapor source−building separation and building construction on soil vapor intrusion as studied with a three-dimensional numerical model, Environ. Sci. Technol. 39 (2005) 4550–4561, https://doi.org/10.1021/es049781k.
[49] Y. Yao, Y. Xiao, F. Mao, H. Chen, I. Verginelli, Examining the role of sub-foundation soil texture in chlorinated vapor intrusion from groundwater sources with a two-layer numerical model, J. Hazard. Mater. 359 (2018) 544–553, https://doi.org/10.1016/j.jhazmat.2018.07.097.
[50] Y. Yao, I. Verginelli, E.M. Suuberg, A two-dimensional analytical model of vapor intrusion involving vertical heterogeneity, Water Resour. Res. 53 (5) (2017) 4499–4513, https://doi.org/10.1002/2016WR020317.
[51] U.S. EPA, Draft guidance for evaluating the Vapor intrusion to indoor air pathway from groundwater and soils (Subsurface Vapor Intrusion Guidance). www.epa.gov (accessed on October 2024), (2002).
[52] U.S. EPA, Regional screening level (RSL) chemical-specific parameters supporting table, 2024. https://www.epa.gov/risk/regional-screening-levels-rsls-generic-tables (accessed on September 2024), (2024).
[53] C. Settimi, I. Verginelli, D. Zingaretti, Examining the role of density-driven transport on chlorinated vapor intrusion, Build. Environ. 266 (2024) 112096, https://doi.org/10.1016/j.buildenv.2024.112096.
[54] U.S. EPA, OSWER technical guide for assessing and mitigating the vapor intrusion pathway from subsurface vapor sources to indoor air, (2015).
[55] U.S. EPA, Vapor intrusion screening level (VISL) calculator user's guide. 2014. https://www.epa.gov/vaporintrusion/visl-users-guide (accessed on March 2025), (2014).
[56] R.W. Falta, I. Javandel, K. Pruess, P.A. Witherspoon, Density-driven flow of gas in the unsaturated zone due to the evaporation of volatile organic compounds, Water Resour. Res. 25 (1989) 2159–2169, https://doi.org/10.1029/WR025i010p02159.
[57] U.S. EPA, National Primary Drinking Water Regulations. https://www.epa.gov/ground-water-and-drinking-water/national-primary-drinking-water-regulations (accessed on May 2025), (2024).
[58] B.H. Kueper, H.F. Stroo, C.M. Vogel, C.H. Ward (Eds.), Chlorinated Solvent Source Zone Remediation, Springer, New York, New York, NY, 2014, https://doi.org/10.1007/978-1-4614-6922-3.
[59] L.D.V. Abreu, H. Schuver, Conceptual model scenarios for the Vapor intrusion pathway. https://www.epa.gov/sites/default/files/2015-09/documents/vi-cms-v11final-2-24-2012.pdf (accessed on July 2025), (2012).
[60] O. Bozkurt, K.G. Pennell, E.M. Suuberg, Simulation of the vapor intrusion process for nonhomogeneous soils using a three-dimensional numerical model, Groundw. Monit. Remediat. 29 (2009) 92–104, https://doi.org/10.1111/j.1745-6592.2008.01218.x.
[61] J.S. Rios Mora, T. Diallo, B. Collignan, M. Abadie, K. Limam, Vapor intrusion in buildings: development of semi-empirical models including lateral separation between the building and the pollution source, Build. Simul. 15 (2022) 2031–2049, https://doi.org/10.1007/s12273-022-0910-3.